An alternate form of probability-distribution plot for D_e values

G. W. Berger

Desert Research Institute, 2215 Raggio Parkway, Reno, NV 89512, USA
(e-mail: glenn.berger@dri.edu)

(Received 17 November 2009; in final form 15 March 2010)

Abstract

The use of probability density distribution (PDD or PD herein) plots for summarizing visually the distributions of paleodose (D_e) values (even when accompanied by a displayed ranking of D_e values) has been criticized over the past decade. Here the suitability of this plot is revisited and an alternate form is proposed for creating a more realistic statistical representation of such data. The alternate plot (TPD, Transformed-PD) is generated by use of a logarithmic transform of D_e values and use of relative, rather than absolute, errors in D_e values. The radial plot also employs such parametric transforms. Examples are given and discussed of distributions of D_e values from both multiple-grain and single-grain SAR (Single Aliquot Regenerative dose) experiments for which a youngest-age interpretation is required. The PD and TPD representations of these data are compared with each other and with the corresponding radial plots. These examples illustrate both the systematic advantages of the TPD plot compared to the conventional PD plot (as heretofore used with D_e data sets) and some limitations of the TPD plot. These limitations can be viewed as either minor or major, depending upon the data set. Generally, the use of the TPD plot (together with ranked D_e values) is an improvement over the comparable use of the PD plot.

Historical context and objective

The PD plot has been used for decades in fission-track (FT) dating (e.g. Hurford et al., 1984; Brandon, 1996) and in $^{40}Ar/^{39}Ar$ (or 'Ar-Ar') dating (e.g. Deino and Potts, 1992; Morgan and Renne, 2008). In these two dating methods PD plots have been used in combination with a superimposed graph of the ranked age estimates and their error bars to represent visually age distributions derived from single-grain analyses. In luminescence dating, the PD plots have been used to display temporal distributions of age estimates from suites of samples within a given geographic region (e.g. Stokes et al., 2004), although Bayesian representations of such temporal distributions may be more valid (e.g. Rhodes et al., 2003). An even broader use of PD plots has been to represent visually detrital zircon (single-grain) age distributions ('age spectra'), to infer episodicity of continental processes (e.g. Condie and Aster, 2009; Condie et al., 2009), usually using data-handling approaches promoted by Sircombe (2004) and Sircombe and Hazelton (2004).

In the last decade PD plots have been employed to replace histograms in the representation of distributions of multiple-grain and single-grain D_e values (e.g. Jacobs et al., 2003; Duller and Augustinus, 2006; Feathers et al., 2006; Berger et al., 2009; Pietsch, 2009; Porat et al., 2009) derived from the SAR (Murray and Wintle, 2003) procedure and its later modifications (e.g., inclusion of IR-wash steps: herein, all modified versions are termed 'SAR'). It therefore seems reasonable to advocate the replacement of the conventional (constant-bin-width) histogram to illustrate dating-result distributions, by some alternate plot so that information on the relative precision of separate ages (FT and Ar-Ar) or D_e values (SAR luminescence) can be presented visually, and so that the presence or absence of relative structure (clustering of data) can be illustrated more effectively.

For some time Galbraith (e.g., 1998, 2005) has advocated replacement of the PD plot in FT dating with the radial plot, based on some sound statistical arguments concerning the generation and propagation of analytical errors in FT age calculations and on other aspects of FT dating. His criticisms of PD plots have been imported into luminescence dating to argue against the use of PD plots for D_e distributions (e.g. Bøtter-Jensen et al., 2003; Lian and Roberts, 2006; Duller, 2008).

The alternate PD plot proposed here minimizes or circumvents the major weakness of the conventional PD plot. The main weakness is the over-emphasis of the statistical significance (relative probability) of

low D_e values in a distribution of a range of D_e values. As shown below, this over-emphasis is caused by two assumptions: that D_e values arise from a statistically Normal (Gaussian) distribution, and that the errors in D_e values are not proportional to the D_e values. The proposed alternate PD plot (when accompanied by ranked D_e values and errors) can communicate more intuitively the relative statistical significance of various apparent components (subpopulations) of the measured D_e values than can the conventional PD plot. That is, the alternate PD plot can quickly and more 'accurately' (in the statistical relative-probability sense) indicate relative structure (or lack of it) in the distribution compared to the conventional PD plot. This alternate PD plot can in turn motivate the selection of various quantitative methods for age calculation. The alternate form of the PD plot does not replace the radial plot as an accurate visual representation of the statistics of each D_e value (when these are greater than zero), but provides for a visually intuitive display of paleodose values (when they are greater than zero). For paleodose values near or less than zero, the conventional PD plot is still useful (e.g. Berger, 2009; Pietsch, 2009), whereas (with D_e values less than zero) the radial plot is not.

Some basic concepts

At the heart of the choice for use or not of the PD plot is consideration of two variables: the appropriateness of the density function (kernel density estimator or kernel) and of the smoothing parameter (bandwidth or data-window width) (e.g. Brandon, 1996; Silverman, 1986; Wand and Jones, 1995). There are many kernel functions (e.g. uniform [or box], triangular, quartic, triweight, biweight, Gaussian, cosine, lognormal, Gamma) in use with various types of data (e.g. Silverman, 1986; Wand and Jones, 1995). While many of these kernels are statistically 'suboptimal' (Wand and Jones, 1995), some such as the Gaussian kernel are not suboptimal by much. Thus, "the choice between kernels can be made on other grounds, such as computational" ease (Wand and Jones, 1995, p. 31). Essentially then, use of a Gaussian kernel is a form of data smoothing. As discussed by several authors (e.g. Silverman, 1986; Wand and Jones, 1995), "smoothing methods provide a powerful methodology for gaining insights into data" (Jones et al., 1996) without highly sophisticated mathematics.

Jones et al. (1996) review the effects of bandwidth choice on smoothing. They show that the Gaussian kernel can over-smooth the density estimate somewhat or 'seriously', depending on the data example. At the other extreme, the shape of the conventional histogram is highly sensitive to the choice of bin width (analogous to bandwidth for kernel density estimators) and of the placement of the bin edges. There are many disadvantages of histograms (e.g. low 'efficiency') compared to kernel estimators (e.g. Wand and Jones, 1995, p.7). An extensive discussion on the use of histograms in Earth Science is provided by Vermeesch (2005).

The appropriateness of bandwidth choice has been discussed in some of the literature concerned with the use of PD plots to represent age spectra for single-grain-zircon (for example) data. A Gaussian function has been deemed apt for representing the kernel of such data. The bandwidth of the Gaussian kernel is based on the standard deviation of each datum. Thus the bandwidth can change at each data point, which provides a distinct improvement over histograms, that employ a constant bin width. However, in (for example) zircon-age-spectra applications (e.g. Condie et al., 2009) bandwidth choice usually comes down to consideration of the age resolution of individual analyses (e.g., 1 Ma or 20 Ma). In the examples and discussion of D_e distributions below, the historic choice of a Gaussian kernel (explicitly defined below) is maintained as this seems to be a reasonable representation of each D_e value derived from multiple-grain and single-grain SAR experiments.

To summarize, this communication outlines how the kernel and bandwidth of PD plots for D_e distributions can be transformed to a more realistic visual and statistical representation of the relative structure in such distributions. Implicitly, there are many experimental variables that affect the statistics of any population of D_e values. Of course deconvolution computational methods (e.g. Minimum Age Model or MAM, Galbraith et al., 1999) may still be required to calculate geologically accurate component D_e values.

Radial and PD plot

Galbraith (1988) introduced the radial plot as "useful for exploratory, diagnostic, or descriptive purposes or to supplement more formal estimation and hypothesis-testing methods". This is essentially the reason others have used the PD plot. Clearly, the radial plot offers advantages over the PD plot, particularly when the PD plot is unaccompanied by a display of ranked data with error bars. In Berger et al. (2009), the PD plot offers these uses (exploratory, diagnostic or descriptive). Those plots motivated the hypothesis-testing exercise of calculating weighted means and standard errors of subsets (for different samples) of D_e values, which in turn led to some accurate youngest age estimates.

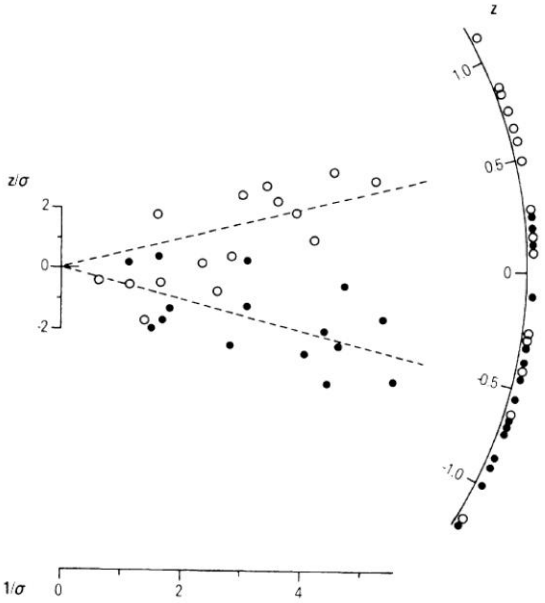

Figure 1: *A radial plot for a mixture of two distinct populations of artificial data (open and filled circles), having distinct means (represented by dashed lines). This is a copy of Figure 3 in Galbraith (1988).*

Galbraith (1988) presented an artificial data set and compared a radial plot and a PD plot to elucidate visually the relative structure in that data set. The data set represented a mixture of two populations, one with mean +0.5 and the other with mean -0.5. In Figure 1 one of these two populations is represented by open circles, the other, by filled circles, and the respective means, by the two dashed lines. Without these graphically displayed distinctions (filled circles and dashed lines), this radial plot merely suggests the existence two populations, but does not clearly resolve them. Plotted as a 'weighted histogram' (a PD plot) in Figure 2, these same artificial data also suggest a bimodal distribution. Inexplicably, Galbraith then states that "the weighted histogram is superficially attractive … but does not point to the true mixture as informatively as Figure 2 does" (his radial plot without filled circles and dashed lines). He makes other qualitative remarks disparaging this PD plot, but it seems that Figure 2 is nearly (or for this data set, 'equally') as informative visually as his radial plot, especially if accompanied by ranked data with error bars. In summary, the PD plot can readily indicate meaningful relative structure, and visualization of such structure can suggest computational hypothesis testing (e.g. calculation of weighted means or use of computational deconvolution methods), depending on the needs of the experiment and the limitations of the data.

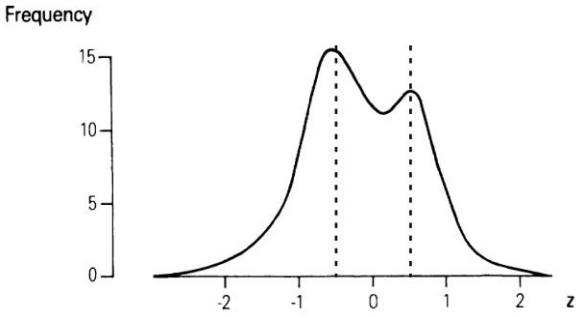

Figure 2: *A modified copy of Figure 9A in Galbraith (1988), showing a 'weighted histogram' plot of the artificial data in Figure 1. I have added dashed lines at the respective known means of the two populations of data.*

Alternate PD-plot formulation

The conventional PD plot of D_e values uses the Gaussian kernel:

$$P_i(D_e) = \frac{1}{\sigma_i\sqrt{2\pi}}\exp\left[-\frac{({}_iD_e - D_e)^2}{2\sigma_i^2}\right] \quad (1)$$

for an aliquot or grain i, having paleodose ${}_iD_e$ and absolute error σ_i. Equation 1 gives the probability of observing a particular D_e value within a range centered on the ${}_iD_e$ value. When summed over all accepted-data i values, equation 1 gives smoothed PD-plot curves. Note that in this form, the sum of $P_i(D_e)$ does not give a 'normalized' probability density, where the sum is divided by the number of items. Singhvi et al. (2001) give an example of a normalized PD plot.

There have been two main criticisms of this conventional PD plot. One is that because for luminescence data the error in D_e is "often proportional to the equivalent dose" (e.g. Duller, 2005, Analyst© Software, Appendix 3), then the PD plot derived from equation 1, using only absolute error estimates, inaccurately represents the relative probabilities of D_e values. It has been recognized for some time (e.g. Berger et al., 1987, Appendix A; Galbraith, 2003) that errors in luminescence data can be constant-relative, not 'absolute'. The second main criticism is that D_e values from SAR data sets are more likely to represent lognormal distributions (e.g., Galbraith et al., 1999; Galbraith, 2003) than Gaussian distributions. The conventional PD plot does not take this distinction into account whereas the radial plot does.

A more technically vague criticism (Galbraith, 1998,

2005, in reference to FT data, but adopted by Bøtter-Jensen et al., 2003, in reference to D_e values) of the use of the conventional PD plots is that "the presence of several estimates with low precision can obscure information, even when there are other high precision estimates in the sample" (Galbraith, 2005, p.195). If this remark is meant to apply only to PD (and other smoothed) plots that lack a companion graph of data points and their error estimates, then it makes sense. Otherwise, this remark applies also to several (most?, any?) pooled estimates, such as the "sound statistical method" (Galbraith, 1988, p.125) of calculating weighted (by inverse variance) means. The use of weighted (by inverse variance) means can be a statistically appropriate tool for some D_e data sets (e.g., Berger et al., 2009; Pietsch, 2009). However, as illustrated with examples below, most D_e data sets probably require a modified form of weighted mean calculation, or use of a central age model or minimum age model calculation.

There are many examples in the literature (e.g. Arnold and Roberts, 2009, and citations therein) for which neither the deconvolution methods nor radial plots are able to 'resolve' meaningful age components, nor do they help resolve 'information' from discretely displayed D_e values. Plotting of ranked D_e values (with errors) together with PD plots certainly 'resolves' individual data points. Thus there are many examples for which smeared distributions of D_e values occur and for which the radial plot does not provide insight into the geological significance of the D_e values. This is probably because there is no geological significance to many such values. These 'smeared' D_e values likely reflect only some unrecoverable grain-transport history, manifesting an interrupted series of daylight exposures somewhere between the start and end of the journey to the final resting place. In this context, it seems then that such technically vague criticisms as mentioned above should be avoided because they can be self-contradictory. Rather, the aforementioned two main criticisms should be addressed. The proposed alternate form of the PD plot is intended at least to minimize the effects of the above two main shortcomings in the PD plots.

The construction of the radial plot (e.g. Galbraith et al., 1999) is based on considerations of the Poisson statistics of luminescence (and FT) measurements, and employs a logarithmic transform. In luminescence, the radial plot assumes that D_e distributions often resemble lognormal distributions. In particular, for luminescence, one can then employ the transforms:

$Z = \ln(D_e)$, $Z_i = \ln({}_iD_e)$, and ${}_R\sigma_i(Z_i) = \sigma_i/{}_iD_e$

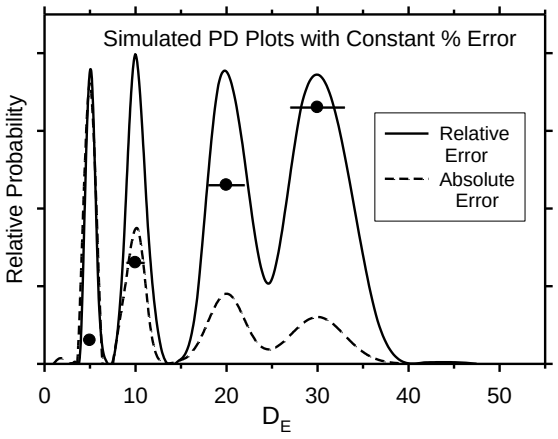

Figure 3: *Relative-probability plots for artificial De data having a constant 10% error (5.0±0.5, 10±1, 20±2, and 30±3 Gy). Here and below, the dashed curve represents the conventional PD plot, which employs equation 1 (see text), and the solid curve represents the TPD plot, employing equation 2 (see text). Here and below, the maxima from each of the separate curves have been scaled roughly (not normalized) to permit easy visualization of their relative structures. This data set is from Appendix 3 of Duller (2005).*

In other words, the ${}_iD_e$ values in equation 1 are replaced by their natural logarithms and the absolute errors are replaced by their corresponding relative errors. As indicated by Galbraith (2003), the appropriate σ would be the standard error of the logarithm of the paleodose, but as he also indicates, this is effectively the relative standard error of the paleodose. When these transformations are applied to equation 1, the alternate (transformed) probability kernel is obtained:

$$T - P_i(Z) = \frac{1}{{}_R\sigma_i\sqrt{2\pi}} \exp\left[-\frac{(Z_i - Z)^2}{2\,{}_R\sigma_i^{\,2}}\right] \quad (2)$$

The resultant summation over all accepted-data aliquots or grains provides the alternate PD plot (a Transformed-PD or TPD plot).

Use of equation 2 instead of equation 1 addresses the criticism of Duller (2005, Analyst© Software, Appendix 3), as shown in Figure 3. Duller gave an example of 4 artificial D_e values all having the same relative error of 10%. He showed that the resultant conventional PD plot (dashed curve in Fig. 3) tends to over-emphasize the relative significance (probability) of the lowest two D_e values. However, application of equation 2 to these same artificial data generates the solid curve in Figure 3, accurately representing their relative probabilities.

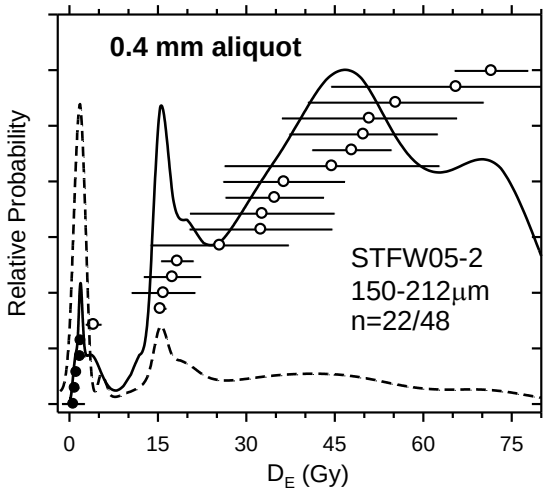

Figure 4: *Relative probability plots, with a ranked series of D_e values and their errors, for a multiple-grain SAR experiment on an irrigation-ditch sediment sample from northern New Mexico (after Berger et al., 2009). Quartz grains of 150-212 µm diameters were employed. Only 22 of 48 aliquots met the standard data-acceptance criteria. Each aliquot contains 10-20 grains.*

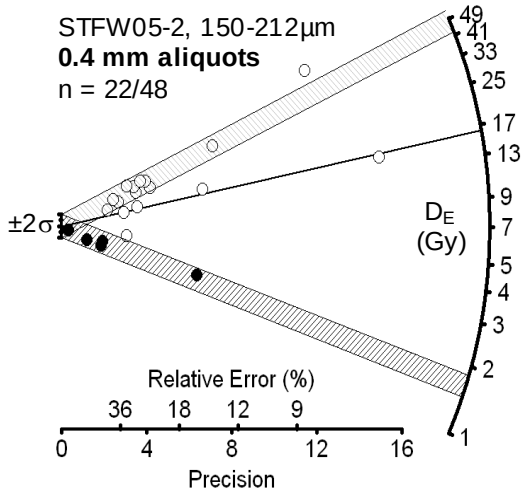

Figure 5: *Radial plot of the data in Figure 4. The center of the ±2 σ lowest bar passes through the weighted mean D_e value derived from the 5 filled-circle data points in Figure 4. For comparison purposes, a thin line is drawn to the approximate center of the peak at ~17 Gy in Figure 4. The ±2 σ top bar is drawn to the approximate center of the broad peak at ~45 Gy in Figure 4.*

It is perhaps worth noting that Brandon (1996) employed a logarithmic transformation and relative errors in his use of the Gaussian kernel, but Galbraith (1998) found fault mainly with Brandon's choice of bandwidth estimation and with the nature of Brandon's error assumptions for FT dating.

It is also worthwhile pointing out that PD plots constructed from ('unlogged') equation 1 can usefully represent D_e distributions containing negative D_e values (e.g. Pietsch, 2009; Fig. 10 in Berger, 2009) such as can arise from analysis of modern-age or very young samples, whereas TPD (and radial) plots cannot represent such D_e data. How can D_e values less than zero arise? An ideal zero-age sample would be expected to produce a distribution of D_e values (e.g., from single grains) described approximately by a Gaussian ('bell curve') centered on $D_e = 0$. Negative values can arise from statistical fluctuations in the luminescence signal within the regions of the shine curves selected for 'signal' and 'background', such that L_0/T_0 can become negative for some grains or aliquots. Not only the TPD plots, but also the usual (logged) deconvolution methods (e.g. MAM and Central-Age-Model or CAM) will fail for distributions containing negative D_e values, as reviewed by Arnold et al. (2009). They conclude that one has to resort to other calculation methods, and suggest use of an 'unlogged' version of MAM. Berger et al. (2009) found that the straightforward use of weighted mean (by inverse variance) D_e values (and standard error of the weighted mean) is sufficiently accurate for their very young samples (e.g. generating a single-grain quartz age estimate of 92.3±9.6 a compared to an historical age of <127 a).

While graphic-representational and computational ambiguity is not uncommon with the use of multiple-grain SAR D_e values (e.g. Arnold and Roberts, 2009), it is also not uncommon with the use of single-grain D_e values, as the examples below illustrate. Rather than reflecting limitations of graphical methods of display or of statistical deconvolution methods of computation, difficulties in interpretation of such data sets more likely reflect unavoidable geological or empirical complexities. For example, positively-skewed 'smeared' single-grain D_e distributions (assuming that each grain hole emits at most a single-grain signal) can merely reflect conditions of non-episodic mixing of grains having arbitrarily different daylight exposure histories. Hopefully, at least the youngest age information can be resolved, graphically or by deconvolution, or by both.

Weighted mean calculations for D_e data

As mentioned, the usual weighted mean calculation (e.g. Topping, 1962) employs weighting by inverse variance of absolute errors. This is appropriate for data having independent errors and for which the

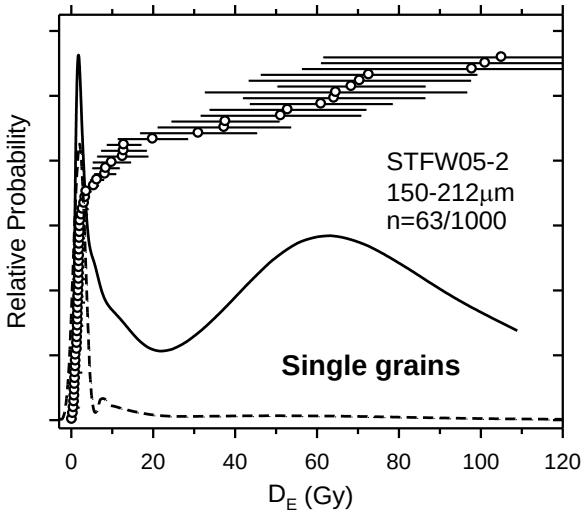

Figure 6: *Relative-probability plots for the single-grain quartz SAR results from the sample in Figure 5. Only 63 of 1000 grain-hole stimulations provided acceptable D_e values using the normal data-acceptance criteria. The small 'wiggle' in the dashed curve at ~6 Gy is an artifact of the spacing of curve-fit data points used for this spline-curve fitting.*

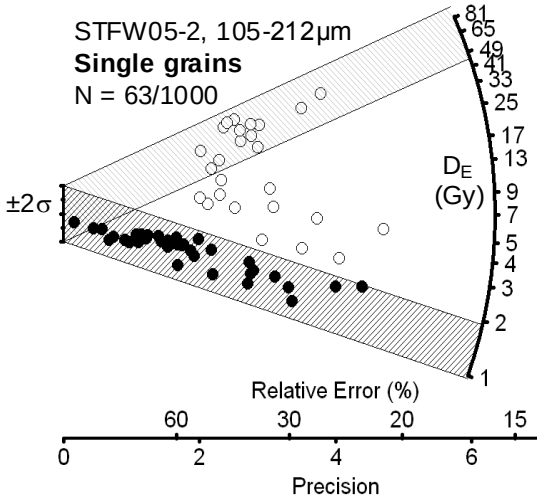

Figure 7: *Radial plot of the data in Figure 6. The $\pm 2\sigma$ lowest bar is centered on the weighted mean calculated for the lowest peak in Figure 6. The $\pm 2\sigma$ top bar is centered at the ~65 Gy peak in Figure 6.*

errors are not clearly proportional to the D_e values. The examples of D_e subsets of Berger et al. (2009) and Pietsch (2009) approximate such data. However, many subset (and whole) D_e distributions (examples below) have errors that are roughly proportional to the D_e values. Moreover, as mentioned above, D_e distributions often resemble lognormal distributions. Therefore, the formulae for calculation of weighted means of D_e values in general should be modified to use $\ln(D_e)$ values and weighting by inverse relative errors. Such a modification or transformation, appropriate for the general statistics of most D_e values, can provide a convenient tool for quick estimates (via spreadsheets) of a mean of a data subset, yet that can be more accurate statistically than the conventional weighted mean calculation. In some of the examples below, this relative error weighted mean (REWM) calculation is employed.

Examples of PD, TPD and radial plots

In the following examples, the PD plot is represented by a dashed line and the TPD plot, by a solid line. Also, the PD and TPD curves are plotted along with ranked D_e values and their 1σ absolute errors. The maximum 'heights' of the PD and TPD plots have been scaled (not normalized) to approximate equivalence for easy visualization of their similarities and differences.

The first example compares the graphical representation by the three plots (PD, TPD, radial) of D_e distributions obtained from both multiple-grain and single-grain SAR experiments on quartz sand from the oldest sample (STFW05-2, historical age $\approx$<450 a) in the study of Berger et al. (2009). D_e values from the use of 0.4 mm aliquots (~10-20 grains each) are shown in Figure 4. Notice that both the PD and TPD plots visually denote a small (5 data points) cluster of D_e values, the weighted (by inverse variance) mean of which was used by Berger et al. (2009) to estimate a minimum age of 487 ± 74 a (from mean D_e = 1.65 ± 0.25 Gy), comparable to the known probable historical age of the sample. However, only the TPD plot draws visual attention to two other (probably geologically meaningless) subgroups of D_e values, one at ~16 Gy and one around 45-50 Gy. This example shows how the TPD plot more realistically represents the relative structure in the population of D_e values than does the conventional PD plot.

In the more accurate statistical representation of these data in a radial plot (Fig. 5), the 3 apparent groups so clearly visualized in the TPD plot are also quite apparent. Though not stated in Berger et al. (2009), the MAM-4 estimate of the youngest-age D_e values in Figure 4 is 2.03 ± 0.28 Gy and the MAM-3 estimate is 1.88 ± 0.45 Gy, neither of which is significantly different from the aforementioned weighted mean of 1.65 ± 0.25 Gy. Incidentally, the REWM estimate for the 5-point cluster of D_e values in Figure 4 is 1.78 ± 0.25 Gy, somewhat closer to the

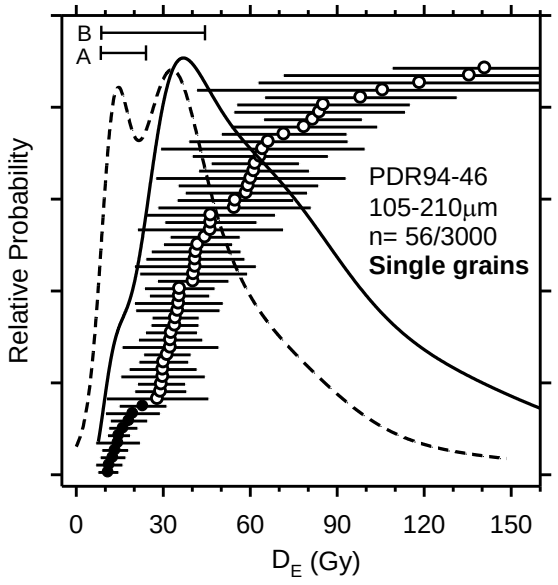

Figure 8: *Relative-probability plots for the single-grain quartz SAR results from a fluvial-sand sample of Antarctica (Berger, unpublished data). Only 56 of 3000 grain-hole stimulations yielded acceptable D_e values (using normal data acceptance criteria). Estimated youngest-age D_e values are presented in the text.*

MAM estimates than is the conventional weighted mean estimate of 1.65 Gy. The main difference between these weighted mean calculations and the MAM calculations is that the MAM models embrace (within 2σ) the sixth data point, shown outside the shaded bar in Figure 5.

The PD and TPD representations of the single-grain quartz D_e values for this sample are shown in Figure 6. It is clear in Figure 6 that of the two plots, only the TPD plot indicates the true statistical significance (relative probability) of several high-value D_e points. This TPD plot also draws more visual attention to the subgroup of D_e values just on the high-side edge of the prominent youngest-age D_e probability peak, thus hinting at the presence of more than one 'Gaussian' there. A comparable visual resolution of the D_e values is attained with the corresponding radial plot (Fig. 7). Thus this single-grain example shows clearly the inadequate visual representation of the relative significances (statistical probabilities) of D_e values provided by the conventional PD plot, and the statistically improved representation with use of the TPD plot.

The second example is of the representation of single-grain quartz D_e data for quartz from fluvial sand in the McMurdo Dry Valleys of Antarctica

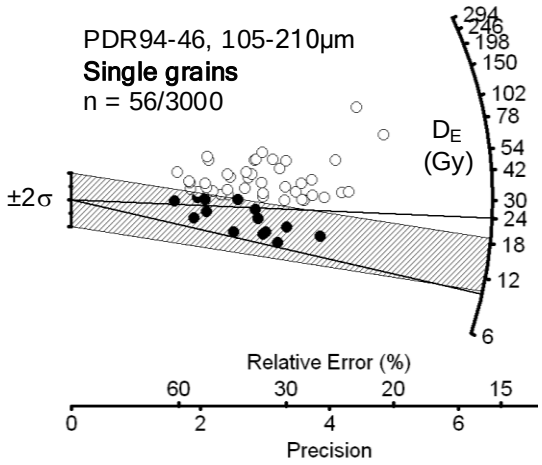

Figure 9: *Radial plot for the data in Figure 8. The $\pm 2\sigma$ bar is centered on the weighted mean D_e value calculated for group A in Figure 8. The two divergent lines span the range of D_e values delimiting group A in Figure 8.*

(Berger, unpublished data). In Figure 8, as in Figures 4 and 6, the TPD plot changes significantly the visual representation of the relative probabilities of the D_e values, and de-emphasizes the lowest D_e values compared to the PD plot. This change appears to lead to a significant ambiguity in estimation of a youngest-age D_e from this data set. On the one hand, the lowest-D_e peak in the PD plot suggests that the filled-circle data (under bar A) could represent a statistically separate subgroup, for which a conventional (inverse variance weighting) weighted mean of 14.0 ± 1.5 Gy (n=10, internal standard error [SE], Topping, 1962) can be calculated. On the other hand, with use of the TPD plot these same data points do not appear to denote a separate subgroup. In this case only a subjectively selected range of D_e values (bar B, upper edge approximately at a slight break near 50 Gy) might yield a geologically useful estimate of a burial or last-daylight age. The conventional weighted mean under bar B is 20.5 ± 1.7 Gy (n=36, external SE). However, close inspection (see D_e values and error bars in Fig. 8) suggests that the REWM calculation is more appropriate. In this case, the REWM under bar A is 14.9 ± 1.6 Gy (internal SE) and under bar B, 28.2 ± 2.0 Gy (external SE). Thus use of the conventional weighted mean can be misleading (bar B) and use of the REWM can be uninformative. In these and all examples, only the largest (most conservative) of the two calculable SE values (Topping, 1962) have been selected. For the data in Figure 8 the MAM-3 estimate of 19.9 ± 3.1 Gy falls between the REWM estimates, and is more appropriate than either.

Thus this example shows that in general for single-grain data sets, the TPD plot is likely to give a more

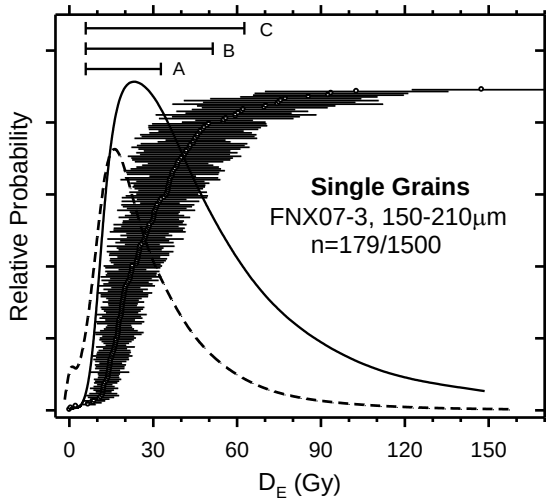

Figure 10: *Relative-probability plots for a fluvial sample from Arizona. The A, B, C groups are discussed in the text. (Berger, unpublished data).*

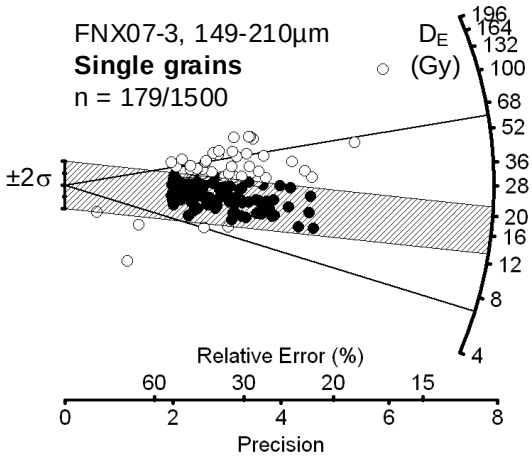

Figure 11: *Radial plot for the data in Figure 10. The ±2σ bar is centered on the weighted mean for group B in Figure 10. The fanned lines span the range of D_e values delimiting group C of Figure 10, used to calculate the group C weighted mean (see text).*

statistically probable visual representation of the distribution of D_e values than would the PD plot, but that statistical methods (e.g., MAM) other than visually-guided weighted mean calculations are likely required to assign confidence to any quantitative estimate of a youngest-age value from such distributions. This is further emphasized in the corresponding radial plot (Fig. 9). Here there is no clear visual resolution of sub-population D_e values, except that which can be estimated by other means (use of either the TPD plot or the MAM computations).

The final single-grain quartz example is from a fluvial deposit in Arizona. In Figure 10, as above, there is a significant difference in visual representation when the TPD plot is employed. Not only is there a significant de-emphasis placed on the contribution of the 3 lowest-D_e values, but also there is an apparently greater ambiguity introduced into the potential choice of D_e values for youngest-age D_e estimation. This example was chosen because it is known that the field-sampling and sample-storage/shipment (by a 'third party') created a laboratory sample for which it was difficult or impossible to exclude all grains that were exposed to daylight during sampling. Thus it is likely that the 3 lowest-D_e data points are 'contaminant' quartz grains, and should be excluded from youngest-age estimation. Certainly they are not feldspar grains.

Unlike in Figures 4 and 6, the TPD plot in Figure 10 (more so than in Fig. 8) provides little or no visual guidance for the selection of subgroups of D_e values for calculation of estimates of the last-daylight-exposure age. While the PD plot might suggest a statistically probable grouping under bar A (delimited roughly by the 50-60%-of-maximum limits of the peak), the TPD plot suggests that the range of this subgroup should be extended to that of either bars B or C. The corresponding conventional weighted means are: 16.1 ± 0.6 Gy (bar A, n=108); 17.6 ± 0.6 Gy (bar B, n=157); and 17.9 ± 0.6 (bar C, n=165). However, as mentioned, the use of REWM is more appropriate for such data (lognormal distribution, similar relative errors). Thus the respective REWM's are: 18.6 ± 0.6 Gy; 22.9 ± 0.8 Gy; and 24.3 ± 0.9 Gy. Excluding the 3 lowest data points, the MAM-3 estimate for this distribution is 17.0 ± 1.7 Gy. This example therefore shows that for such a distribution the MAM provides probably the most statistically accurate estimate for the youngest-age grouping of D_e values, but that the TPD main peak can denote visually roughly where the youngest-age estimate may be. In this case, a REWM estimate for a subgroup (bar A) of D_e values close to the 'half-Gaussian' (peak low-side, e.g., Pietsch, 2009) part of the TPD peak (the peak is asymmetrical) is comparable to the MAM estimate.

Thus in this example, considerations of both the details of the sample-handling history and of the deconvolution approach are necessary for appropriate interpretation of embedded youngest-age information. These inferences are affirmed by the corresponding radial plot (Fig. 11). Here also an appropriate interpretation requires use of either the MAM computation or guidance from a TPD plot,

preferably the former, but coupled with before-hand knowledge of imperfections in field sampling.

In this context of the complexities of interpretation of D_e distributions and of the topic of field-sample contamination, consideration of the effects on such distributions of the details of field sampling may be worth examining in the future. There are many examples of the presence of inexplicably 'too-young' D_e values in radial plots (e.g., Jacobs et al., 2008a, 2008b). While unaccounted effects of micro-dosimetry may contribute to this presence, perhaps the use of 'brute-force' tube-sampling methods may also contribute via unobserved translocation of daylight-exposed grains into the interior length of the tubes. More attention needs to be directed to this aspect of single-grain dating.

Conclusions

The proposed transformed (using logarithms and relative error estimates) form of the conventional (unlogged) PD plot addresses the perceived main shortcomings of the PD plot when displaying D_e distributions. The Transformed-PD (TPD) plot, employing the same parametric transforms as used in the radial plot, can place a statistically more realistic emphasis on the higher-D_e data points. That is, like the radial plot, it also reveals meaningful relative structure in D_e distributions, providing a display which can motivate the selection of quantitative methods for age calculation. Moreover, the TPD plot (accompanied by ranked D_e values and error estimates) is visually easy to understand, especially when dealing with 'partial-bleaching' (mixed age) populations for which a youngest-age estimate is required. Motivated by such plots, selection of D_e values for age estimation can vary from use of the straightforward calculation of weighted means with standard errors (e.g. Topping, 1962) to the use of more sophisticated methods such as the minimum-age, central-age or mixed-age models (Galbraith et al., 1999; Arnold et al., 2009). However, for many groupings of D_e values, transformed weighted mean calculations (using relative errors and $\ln[D_e]$ values) are more appropriate than are conventional weighted mean calculations.

Because the TPD plot employs a logarithmic transform of D_e values, this plot (and the radial plot) cannot be used, unlike the PD plot, to represent D_e distributions having negative values, such as are routinely encountered with modern-age or very young samples. For those samples, the PD plot is still useful for visual representation of the relative structure of the D_e distribution and for selection of an appropriate subset of D_e values for use in weighted mean calculation (e.g. Berger, 2009) or use in another approach (Pietsch, 2009). These subset calculations in turn can provide sufficiently accurate estimates of a youngest age. For either type of plot, it remains important to display concurrently a ranked series of D_e values with their estimated errors.

In this presentation, it is implicit that a 'one-size-fits-all' style of graphical display of D_e distribution data is unsuited to the variety of data likely to be generated from geological settings.

Acknowledgements and postscript

I thank Dr. Ashok Singhvi for careful comments that helped me to clarify this presentation. A spreadsheet form of TPD-curve-data calculation is available from the author. It will generate data suitable for plotting smooth curves via other software.

References

Arnold, L.J., Roberts, R.G. (2009) Stochastic modelling of multi-grain equivalent dose (D_e) distributions: Implications for OSL dating of sediment mixtures. *Quaternary Geochronology* **4**, 204-230

Arnold, L.J. Roberts, R.G., Galbraith, R.F., DeLong, S.B. (2009) A revised burial dose estimation procedure for optical dating of young and modern-age sediments. *Quaternary Geochronology* **4**, 306-325.

Berger, G.W. (2009) Zeroing Tests of Luminescence sediment dating in the Arctic Ocean: Review and new results from Alaska-margin core tops and central-ocean dirty sea ice. *Global and Planetary Change* **68**, 48-57.

Berger, G.W., Post, S., Wenker, C. (2009) Single and multigrain quartz luminescence dating of irrigation-channel features in Santa Fe, New Mexico, *Geoarchaeology* **24**, 383-401.

Berger, G.W., Lockhart, R.A., Kuo, J. (1987) Regression and error analysis applied to the dose response curves in thermoluminescence dating. *Nuclear Tracks and Radiation Measurements* **13**, 177-184.

Bøtter-Jensen, L., McKeever, S.W.S., Wintle, A.G. (2003) *Optically Stimulated Luminescence Dosimetry*, 350 pp., Elsevier, Amsterdam.

Brandon, M.T. (1996) Probability density plot for fission-track grain-age samples. *Radiation Measurements* **26**, 663-676.

Condie, K.C., Aster, R.C. (2009) Zircon age episodicity and growth of continental crust. *Eos Trans. Amer. Geophys. Union* **90**, 364.

Condie, K.C., Belousova, E., Griffin, W.L., Sircombe, K.N. (2009) Granitoid events in space and time: Constraints from igneous and

detrital zircon age spectra. *Gondwana Research* **15**, 228-242.

Deino, A., Potts, R. (1992) Age-probability spectra for examination of single-crystal $^{40}Ar/^{39}Ar$ dating results: Examples from Olorgesailie, Southern Kenya Rift. *Quaternary International* **13/14**, 47-53.

Duller, G.A.T. (2005) *Analyst, v.3.22b*, University of Wales, 43p.

Duller, G.A.T. (2008) Single grain optical dating of Quaternary sediments: why aliquot size matters in luminescence dating. *Boreas* **37**, 589-612.

Duller, G.A.T., Augustinus, P.C. (2006) Re-assessment of the record of linear dune activity in Tasmania using optical dating. *Quaternary Science Reviews* **25**, 2608-2618.

Feathers, J.K., Holliday, V. T., Meltzer, D.J. (2006) Optically stimulated luminescence dating of Southern High Plains archaeological sites. *Journal of Archaeological Science* **33**, 1651-1665.

Galbraith, R.F. (1988) Graphical display of estimates having differing standard errors. *Technometrics* **30**, 271-281.

Galbraith, R.F. (1998) The trouble with probability density plots of fission-track ages. *Radiation Measurements* **29**, 125-131.

Galbraith, R.F. (2003) A simple homogeneity test for estimates of dose obtained using OSL. *Ancient TL* **21**, 75-77.

Galbraith, R.F. (2005) *Statistics for Fission Track Analysis*, 224 pp., Chapman and Hall/CRC, Boca Raton, USA.

Galbraith, R.F., Roberts, R.G., Laslett, G.M., Yoshida, H., Olley, J.M. (1999) Optical dating of single and multiple grains of quartz from Jinmium rock shelter, northern Australia: part I, experimental design and statistical models. *Archaeometry* **41**, 339-364.

Hurford, A.J., Fitch, F.J., Clarke, A. (1984) Resolution of the age structure of the detrital zircon populations of two Lower Cretaceous sandstones from the Weald of England by fission track dating. *Geology Magazine* **121**, 269-277.

Jacobs, Z., Duller, G.A.T., Wintle, A.G. (2003) Optical dating of dune sand from Blombos Cave, South Africa: II—single grain data. *Journal of Human Evolution* **44**, 613-625.

Jacobs, Z., Wintle, A.G., Duller, G.A.T., Roberts, R.G., Wadley, L. (2008a) New ages for the post-Howiesons Poort, late and final Middle Stone Age at Sibudu, South Africa. *Journal of Archaeological Science* **35**, 1790-1807.

Jacobs, Z., Wintle, A.G., Roberts, R.G., Duller, G.A.T. (2008b) Equivalent dose distributions from single grains of quartz at Sibudu, South Africa: Context, causes and consequences for optical dating of archaeological deposits. *Journal of Archaeological Science* **35**, 1808-1820.

Jones, M.C., Marron, J.S., Sheather, S.J. (1996) A brief survey of bandwidth selection for density estimation. *Journal of the American Statistical Association* **91**, 401-407.

Lian, O.B., Roberts, R.G. (2006) Dating the Quaternary: progress in luminescence dating of Sediments. *Quaternary Science Reviews* **25**, 2449-2468.

Morgan, L.E., Renne, P.R. (2008) Diachronous dawn of Africa's Middle Stone Age: New $^{40}Ar/^{39}Ar$ ages from the Ethiopian Rift. *Geology* **36**, 967-970.

Murray, A.S., Wintle, A.G. (2003) The single-aliquot regenerative dose protocol: potential for improvements in reliability. *Radiation Measurements* **37**, 377-381.

Pietsch, T.J. (2009) Optically stimulated luminescence dating of young (<500 years old) sediments: Testing estimates of burial dose. *Quaternary Geochronology* **4**, 406-422.

Porat, N., Duller, G.A.T., Amit, R., Zilberman, E., Enzel, Y. (2009) Recent faulting in the southern Arava, Dead Sea Transform: Evidence from single-grain luminescence dating. *Quaternary International* **199**, 34-44.

Rhodes, E.J., Bronk Ramsey, C., Outram, Z., Batt, C., Willis, L., Dockrill, S., Bond, J., (2003) Bayesian methods applied to interpretation of multiple OSL dates: high precision sediment ages from Old Scatness Broch excavations, Shetland Islands. *Quaternary Science Reviews* **22**, 1231-1244.

Silverman, B.W. (1986) *Density Estimation for Statistics and Data Analysis*. 175 pp. Chapman and Hall, London, UK.

Singhvi, A., Bluszcz, A., Bateman, M.D., Rao, M.S. (2001) Luminescence dating of loess-paleosol sequences and coversands: methodological aspects and paleoclimatic implications. *Earth Science Reviews* **54**, 193-211.

Sircombe, K.N. (2004) AgeDisplay: an EXCEL workbook to evaluate and display univariate geochronological data using binned frequency histograms and probability density distributions. *Computers & Geosciences* **30**, 21-31.

Sircombe, K.N., Hazelton, M.L. (2004) Comparison of detrital age distributions by kernel functional estimation. *Sedimentary Geology* **171**, 91-111.

Stokes, S., Bailey, R.M., Fedoroff, N., O'Marah, K.E. (2004) Optical dating of aeolian

dynamism on the West African Sahelian margin. *Geomorphology* **59**, 281-291.

Topping, J. (1962) *Errors of Observation and their Treatment*. 116 pp., Chapman and Hall, London.

Vermeesch, P. (2005) The statistical uncertainty associated with histograms in the Earth Sciences. *Journal of Geophysical Research* **110**, B02211.

Wand, M.P., Jones, M.C. (1995) *Kernel Smoothing*. 207 pp. Chapman and Hall, London, UK.

Reviewer

A.K. Singhvi